NEOPLASIA
www.neoplasia.com
Volume 21 Number 11 November 2019 pp. 1085–1090

Original Research

Extracellular acidosis differentiates pancreatitis and pancreatic cancer in mouse models using acidoCEST MRI

Rachel A. High[a]; Edward A. Randtke[b]; Kyle M. Jones[c]; Leila R. Lindeman[a]; Jacqueline C. Ma[d]; Shu Zhang[d]; Lucia G. LeRoux[d]; Mark D. Pagel[d]

[a]Cancer Biology Interdisciplinary Program, University of Arizona, Tucson, AZ, USA; [b]Department of Medical Imaging, University of Arizona, Tucson, AZ, USA; [c]Department of Biomedical Engineering, University of Arizona, Tucson, AZ, USA; [d]Department of Cancer Systems Imaging, University of Texas MD Anderson Cancer Center, Houston, TX, USA

Abstract

Differentiating pancreatitis from pancreatic cancer would improve diagnostic specificity, and prognosticating pancreatitis that progresses to pancreatic cancer would also improve diagnoses of pancreas pathology. The high glycolytic metabolism of pancreatic cancer can cause tumor acidosis, and different levels of pancreatitis may also have different levels of acidosis, so that extracellular acidosis may be a diagnostic biomarker for these pathologies. AcidoCEST MRI can noninvasively measure extracellular pH (pHe) in the pancreas and pancreatic tissue. We used acidoCEST MRI to measure pHe in a KC model treated with caerulein, which causes pancreatitis followed by development of pancreatic cancer. We also evaluated the KC model treated with PBS, and wildtype mice treated with caerulein or PBS as controls. The caeruleintreated KC cohort had lower pHe of 6.85–6.92 before and during the first 48 h after initiating treatment, relative to a pHe of 6.92 to 7.05 pHe units for the other cohorts. The pHe of the caeruleintreated KC cohort decreased to 6.79 units at 5 weeks when pancreatic tumors were detected with anatomical MRI, and sustained a pHe of 6.75 units at the 8week time point. Histopathology was used to evaluate and validate the presence of tumors and inflammation in each cohort. These results showed that acidoCEST MRI can differentiate pancreatic cancer from pancreatitis in this mouse model, but does not appear to differentiate pancreatitis that progresses to pancreatic cancer vs. pancreatitis that does not progress to cancer.

Neoplastic (2019) 21, 1085–1090

Introduction

Pancreatic cancer (PC) prevalence has been increasing over several decades, despite advances in testing and treatment methods [1–3]. Due to a lack of early stage physical symptoms and specific diagnostic biomarkers, most PCs go undetected until progression into latestage disease [4]. Indeed, fewer than 15% of PCs are resectable by the time of diagnosis, reinforcing the need for biomarkers or predictive tests to evaluate PC risk [5]. While acute and chronic pancreatitis have been shown to be risk factors for pancreatic cancer development [6–11], there is currently no way to distinguish the atrisk subpopulation of patients who will ultimately develop PC from those patients whose pancreatitis will resolve or maintain with no progression to cancer [11,12]. The lack of screening for the patients in this atrisk subpopulation can delay identification of their cancer by up to two years [11], reducing the likelihood that detected cancers will be resectable and respond well to treatment. The disconnect between known risk factors and time of diagnosis reinforces the need for noninvasive screening methods that can detect early neoplastic changes.

Acidosis in the extracellular tumor microenvironment is a common characteristic of most solid tumors [13]. While a definitive biological reason is unclear, cancer cells typically metabolize glucose to lactate via aerobic glycolysis, a phenomenon known as the Warburg effect [14,15]. Excess intracellular lactate and H^+ ions resulting from this process are ultimately secreted from the cell, causing acidification in the extracellular tumor

Abbreviations: CEST, chemical exchange saturation transfer, KC, $Kras^{LSL.G12D/+}$, PdxCre, mouse model, MRI, magnetic resonance imaging

Corresponding author at: Department of Cancer Systems Imaging, University of Texas MD Anderson Cancer Center, 1881 East Road, 3SCR4.3642, Houston, TX 77054, USA.
e-mail address: mdpagel@mdanderson.org (M.D. Pagel).

Received 18 April 2019; received in revised form 26 September 2019; accepted 30 September 2019

https://doi.org/10.1016/j.neo.2019.09.004

microenvironment relative to normal tissues [16]. Thus, extracellular pH (pHe) can be used as a biomarker of cancer detection. Assessments of pHe have been shown to differentiate tumor from healthy tissue in a variety of cancer types, including mouse models of pancreatic ductal adenocarcinoma (PDAC) [17].

While a variety of methods exist for *in vivo* pH measurement, such as PET, optical imaging, and MR spectroscopy, these methods are limited by imaging depth, spatial resolution, and/or a semiquantitative nature [18]. These issues are improved by chemical exchange saturation transfer magnetic resonance imaging (CEST MRI), one of the first noninvasive imaging techniques that can accurately and precisely measure pHe *in vivo* [19,20]. CEST MRI is a method by which the coherent magnetic resonances of labile protons in exogenous or endogenous compounds are selectively saturated, followed by exchange of the protons with water, which causes a decrease in the water MRI signal (Figure 1A). Because the exchange of these saturated protons with protons in water molecules is basecatalyzed, the resultant CEST signal amplitude is pHdependent (Figure 1B). AcidoCEST MRI is a subset of this method that uses an exogenous CT agent that has been repurposed for MRI, which has been used for *in vivo* pHe measurements both preclinically and clinically [21–28]. Our study evaluated the efficacy of acidoCEST MRI in pHe detection of spontaneous murine PC.

The determination of pHe in PC is further complicated by its inflammatory nature. One common method of identification and staging of cancer, [18F]fluorodeoxyglucose positron emission tomography (FDGPET), can be confounded by the presence of inflammation, as both inflammation and malignant tumors have increased glucose uptake [29,30]. Inflammation is known to lower pHe, although this decrease in pHe is expected to be mild. Therefore, we hypothesized that inflammation of the pancreas, or pancreatitis, causes only a mild decrease in tissue pHe, while PC has a lower pHe than pancreatitis. Furthermore, previous studies with acidoCEST MRI have not evaluated the overall effect of inflammation on tissue pHe. Therefore, we also hypothesized that acidoCEST MRI can measure a statistically significant difference in pHe between pancreatitis and PC.

In this preliminary study, we sought to investigate the ability of acidoCEST MRI to detect PDAC in the presence of an inflammatory background. To perform this study, we induced pancreatitis in a KC model through treatment with caerulein, which evolves to form pancreatic tumors [31,32]. We also induced pancreatitis in wildtype mice as a control. We measured *in vivo* pHe prior to caerulein treatment, during pancreatitis, and during the development of PDAC. We evaluated our results to determine if acidoCEST MRI can distinguish PDAC from pancreatitis, and whether acidoCEST MRI can prognosticate pancreatitis that progresses to pancreatic cancer.

Material and methods

Mouse models

Male and female C57BL/6J mice (WT) (The Jackson Laboratory, Bar Harbor, ME, USA) and $Kras^{LSL.G12D/+}$; PdxCre (KC) mice were used for all studies, as prepared by the Experimental Mouse Shared Resource of the University of Arizona Cancer Center, Tucson, AZ. To induce pancreatic inflammation, 10 week old WT and KC mice were injected intraperitoneally into the lower right quadrant with 50 g/kg/bw of caerulein (SigmaAldrich, St. Louis, MO, USA) dissolved in PBS for a 100 L total injection volume. Caerulein aliquots for mouse dosing were diluted from a stock solution of 100 g/mL caerulein in PBS. Mice were made to fast for 12 h prior to injections and were injected with hourly intervals of 7 doses, followed by 48 h of rest and 7 additional hourly injections. KC mice that were injected with caerulein developed pancreatic tumors within 5 weeks.

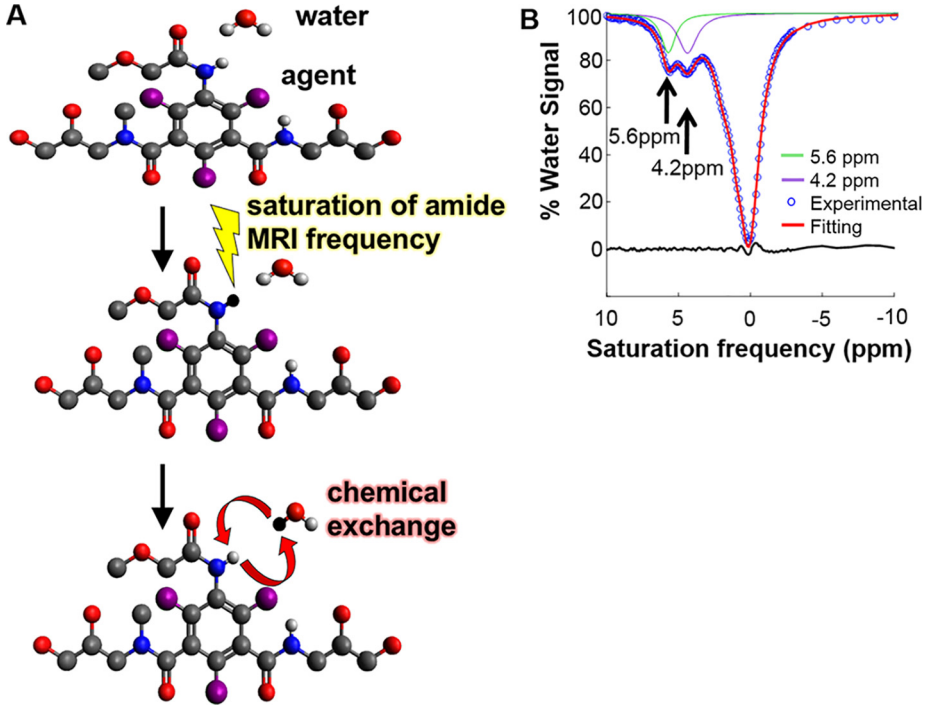

Figure 1. The mechanism of CEST MRI. Iopamidol, a CT agent repurposed for acidoCEST MRI measurements of pH, is shown in this figure. A) Selective saturation of the MRI frequency of an amide proton causes the loss of net coherent MRI signal from the proton. Subsequent chemical exchange of the amide proton with a proton on water causes the saturation to be transferred to the water. B) A Z-spectrum, also known as a CEST spectrum, is generated by selectively saturating MRI frequencies and detecting the coherent water MRI signal amplitude.

A total of 5, 5, 3, and 11 mice were used for the PBStreated wild type, caeruleintreated wildtype, PBStreated KC, and caeruleintreated KC cohorts, respectively. A greater number of mice in the caerulientreated KC chort was used to anticipate potential mouse death before the end of the study due to pancreatic tumor load.

Mice were anesthetized with 1–3% isofluorane in 1 L/min oxygen gas prior to imaging, and maintained at 1.5–2.0% isoflurane during imaging. To deliver the contrast agent bolus and infusion, a tail vein was catheterized with a 27 gauge needle, which was attached to an injection line that extended outside the MRI magnet. Mouse body temperature was monitored using a fiberoptic rectal probe and was maintained at 37 0.5 C. Mouse respiration was monitored using a pneumatic sensor and was maintained between 30 and 50 breaths per minute.

MRI acquisitions

MRI scans were performed with a 7 T Bruker Biospec MRI scanner with a 20 cm bore and 72 mm transceiver volume coil (Bruker Biospin, Inc., Bilarica, Massachusetts, USA). Anatomical images were first acquired to locate the pancreas using a MultiSlice MultiEcho (MSME) MRI acquisition method, with a 2000 ms repetition time, 10.36 ms effective echo time, 128x96 matrix size, 6.4x4.8 cm field of view, 453x453 m^2 inplane resolution, and 1 mm slice thickness. All anatomical MR images were performed using respiration gating to minimize motion artifacts.

AcidoCEST MR images of the pancreas were then acquired with four repetitions of the a CESTFISP pulse sequence, followed by intravenous injection of 200 L of 370 mg of iodine per mL of iopamidol (Isovue, Bracco Imaging S.p.A., Milan, Italy). The injection line was then connected to an infusion pump which delivered 400 L/h of contrast agent for the remainder of the scanning period. After contrast agent bolus injection and during contrast agent infusion, mice were scanned with six repetitions of the acidoCEST MRI sequence. All acquisitions of the acidoCEST sequence had a 4.16 ms repetition time, 1.88 ms echo time, a 128 96 matrix size, 6.4 4.8 cm field of view, 453 453 m^2 inplane resolution, 2 mm slice thickness, 6 s CEST saturation time, 3.5 T saturation power, and continuous wave, rectangular pulse shape, iteratively applied at 40 saturation frequencies. All acidoCEST MR images were performed using respiration gating to minimize motion artifacts as previously reported [26,27].

MRI analyses

AcidoCEST MR images were analyzed using previously established methods [20,26]. Briefly, preinjection images at the same saturation frequency were averaged and the signaltonoise ratio was improved with Gaussian spatial smoothing. Postinjection images were processed using the same procedure. The averaged preinjection images were subtracted from the averaged postinjection images at the same saturation frequency to eliminate endogenous CEST signals. The resulting CEST spectra for each pixel were fit with the BlochMcConnell equations that were modified to include pH as a fitting variable. Pixels with contrast above 22 multiplied by the standard deviation of scan noise were considered to have a 95% probability of representing the contrast agent. Additionally, only pHe values inside the range of 6.3–7.4 pH units were included in the mapping, as analysis of phantom data proved measurements within this range to be most reliable. Statistical significance, or the absence of this significance, was evaluated using a Students twotailed ttest with equal variance. A value of p 0.05 was considered to be statistically significant.

Immunohistochemistry

Upon completion of imaging, mice were sacrificed and pancreases were harvested. Tissue was fixed in 10% buffered formalin for 12 h before transfer to 70% ethanol. Tissue was then embedded in paraffin and processed with the Leica ASP6025 Automatic Tissue Processor (Leica Biosystems, Buffalo Grove, IL, USA) for IHC. Tissue was cut in 3 m thick sections. A total of 8, 12, 8, and 15 tissue samples were stained for the PBStreated wild type, caeruleintreated wildtype, PBStreated KC, and caeruleintreated KC cohorts, respectively. Tissues were stained with antiKi67, antiCD45, or antiCK19 antibodies (Abcam, Cambridge, MA, USA), which indicate neoplasia, inflammation, and ductal hyperplasia, respectively. Digital micrographs were captured using a widefield light microscope (AxioZoom16 (AZ16), Zeiss Microscopy, Jena, Germany). Histology for all cohorts was conducted after the 5 week imaging time point.

Results

We used a T_2weighted, anatomical MRI to localize the pancreas and pancreatic tumors (Figure 2). A 10.36 ms effective echo time enhanced the T_2 weighting of the image contrast, which improved the tissue visualization. To improve the contrasttonoise (CNR) of the acidoCEST MR images, we acquired four CEST image sets prior to injection and six image sets after injection, which required 30–40 min, in which the exact time depended on the breathing rate of the mouse due to the need for prospective respiratory gating (Figure 3). Only 5% of the 40 acidoCEST MRI scans performed with WT mice did not yield usable data, primarily due to motion artifacts that were not adequately suppressed by respiratory gating. For comparison, 12% of the acidoCEST MRI scans performed on KC mice did not yield usable data, primarily due to mouse death while being imaged under anesthesia. Mice with a heavy tumor load were particularly susceptible to death under anesthesia, especially caeruleintreated KC mice in weeks 5 and 8. To reduce the burden of multiple imaging timepoints on these mice, not all the mice imaged at 8 weeks were imaged at 5 weeks. The numbers of successful acidoCEST MRI scans for each

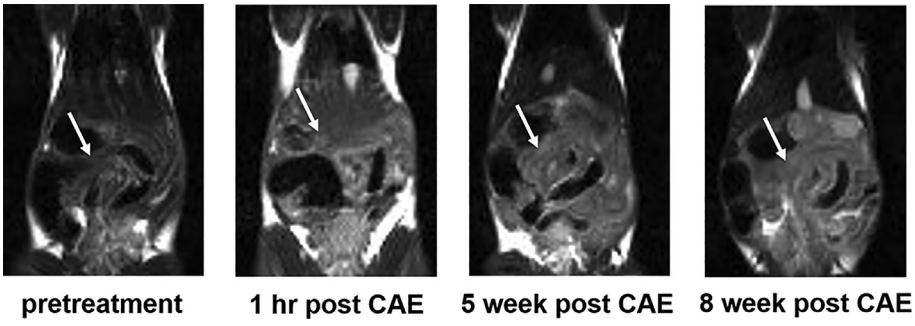

Figure 2. Anatomical MRI localized the pancreas and pancreatic tumors. A MSME MRI acquisition method with a 10.36 msec effective TE resolved the pancreas and pancreatic tumor in a KC model treated with caerulein, as highlighted with a white arrow.

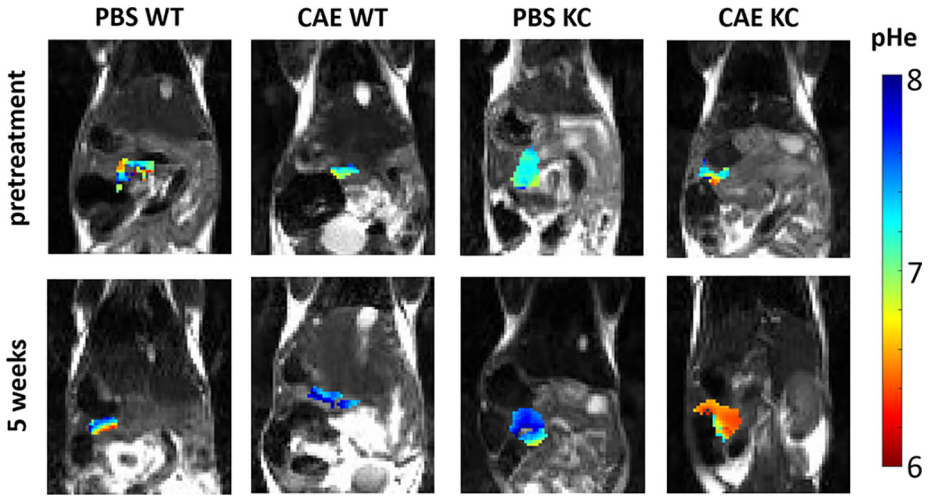

Figure 3. Parametric maps of pHe. Parametric maps are shown at pretreatment and at 5 weeks post-treatment for the PBS-treated wild-type (PBS WT), caerulein-treated wild-type (CAE WT), PBS-treated KC (PBS KC), and caerulein-treated KC (CAE KC) cohorts.

cohort at each time point are listed in Figure 4, relative to the 5, 5, 3, and 11 mice that were used for the PBStreated wild type, caeruleintreated wildtype, PBStreated KC, and caeruleintreated KC cohorts, respectively.

AcidoCEST MRI measured average pHe values that were not significantly different before treatment with PBS or caerulein in the WT and KC models (Figure 4). The average pHe did not significantly change over time for the PBStreated WT, caeruleintreated WT, or PBStreated KC cohorts. The average pHe values of these three cohorts had a narrow range from 6.92 to 7.05 pHe units (except for the caeruleintreated WT cohort that had an average pHe of 6.85 units). For comparison, the caeruleintreated KC cohort had an average pHe of 6.85 to 6.92 before and during the first 48 h of treatment, followed by a decrease to 6.79 units at 5 weeks when pancreatic tumors were detected with anatomical MRI. This lower pHe was sustained at the 8week time point, with an average pHe value of 6.75 units. Due to the standard deviation of these measurements that ranged between 0.4 and 0.21 pHe units, and the relative low number of successful acidoCEST MRI scans of pancreatic tumors, this decrease in pHe observed in pancreatic tumors was not statistically significant relative to pHe measurements made at earlier time points with this cohort, or relative to other cohorts at the 5week time point.

Histopathological validation showed that the WT mice treated with PBS or caerulein did not have pancreatic tumors (Figure 5). These cohorts

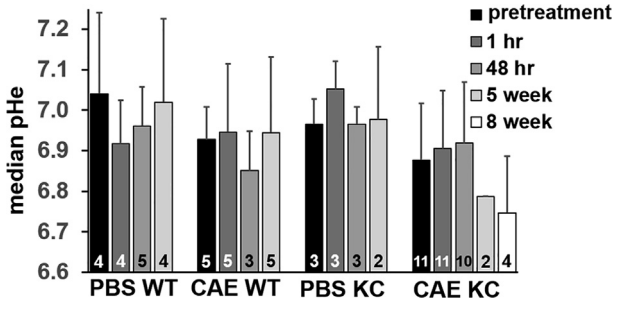

Figure 4. Average pHe measurements. The mean pHe value of each mouse was measured, and the mean and standard deviation of the mice in each cohort was then plotted in the histogram, for PBS-treated wild-type (PBS WT), caerulein-treated wild-type (CAE WT), PBS-treated KC (PBS KC), and caerulein-treated KC (CAE KC) cohorts. Error bars represent the standard deviation. The number of values for each average and standard deviation are listed on each histogram bar.

displayed a lack of Ki67 stain for high cell proliferation or CK19 stain for ductal tumor cells. Instead, these WT cohorts showed evidence for inflammation due to CD45 staining at 5 weeks after treatment. Histopathology showed evidence of high cell proliferation, ductal cell morphology, and inflammation in both the PBStreated and caeruleintreated KC cohorts. The high cell proliferation and ductal cell morphology in the caeruleintreated KC cohort correlated with the presence of pancreatic tumors detected by MRI. The high cell proliferation, ductal cell morphology, and inflammation detected with histopathology in the PBStreated KC cohort were unexpected, because anatomical MRI did not detect pancreatic tumors in this cohort.

Discussion

In this preliminary study, we showed that acidoCEST MRI can measure pHe in the pancreas and in pancreatic tumors. AcidoCEST MRI requires a high concentration of iopamidol to be delivered to tissues and tumors, estimated to be 7–10 mM at 7 T magnetic field strengths based on our past Blochfitting analyses that include concentration as a fitting parameter [20,26]. We show that a sufficient concentration of agent was delivered to pancreas tissues in a variety of disease states for pHe measurements with acidoCEST MRI.

Our results showed that acidoCEST MRI can distinguish pancreatitis from PDAC in this murine model. However, our studies were not able to differentiate between pancreatitis in WT mice that subsequently resolved and pancreatitis in KC mice that progressed to PDAC, suggesting that tumor pHe is not a biomarker that can predict the progression of pancreatitis to PDAC. Follow up studies with pHe measurements and histology at additional early time points could further interrogate differences between models of pancreatitis that do and do not progress to PDAC. Additionally, other inflammatory models of cancer could be compared to these results from our studies of PDAC.

Several difficulties in using this method to measure pH in the pancreas became apparent during this study. Primarily, acidoCEST MRI was not able to detect tumors in untreated KC mice, despite histology showing the presence of lesions. This may be due to the small size of the pancreatic lesions, which may have been in an early disease state relative to lesions in the treated KC mice. Difficulty locating smaller lesions was complicated by the limited spatial resolution of small animal MRI [19]. In future studies, improved resolution may facilitate the selection of the region of interest (ROI) in the images that represent the pancreas and pancreatic tumor.

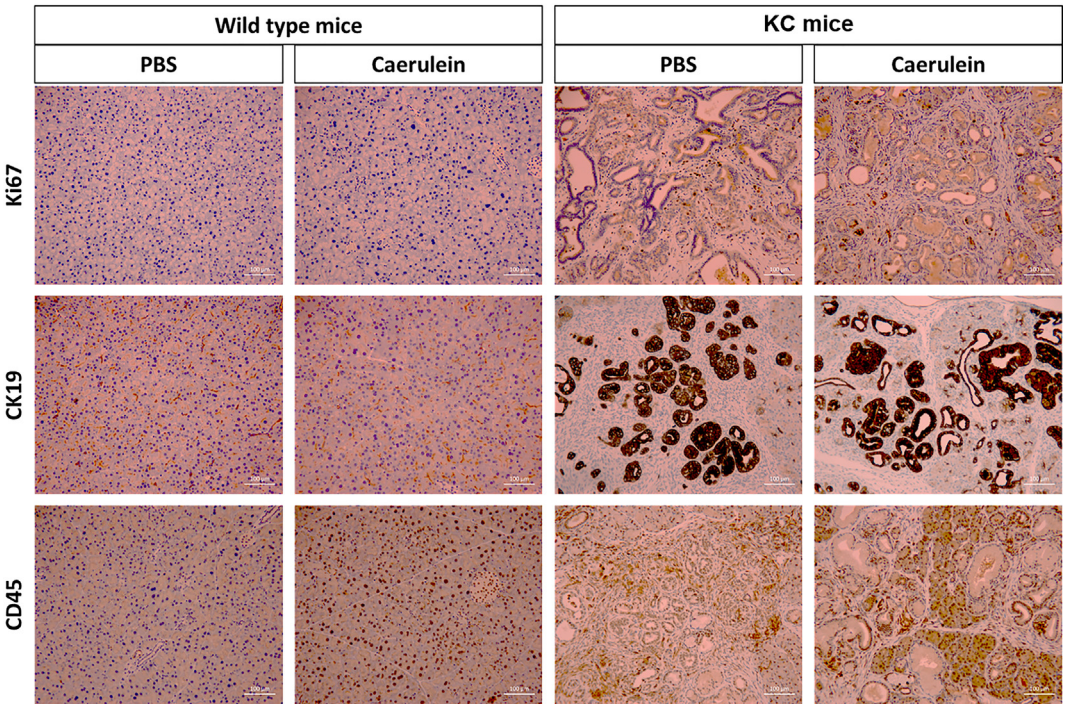

Figure 5. Histopathological validation of the treated models. Ki67 staining was used to evaluate cell proliferation. CK19 staining was used to identify duct cells. CD45 staining was used as an indicator of inflammation. The wild type mice showed no evidence for tumors or inflammation. Caerulein-treated KC mice showed evidence for pancreatic tumors and inflammation, which matched the presence of pancreatic tumors detected with MRI. PBS-treated KC mice showed evidence for high cell proliferation, ductal cell morphology, and inflammation, despite the absence of pancreatic tumors detected with MRI.

Additionally, our acidoCEST MRI method used a slice thickness of 2 mm, which may cause partial volume effects in which a 3D voxel contains a mixture of tissue types, such as healthy and diseased tissue. Improving the contrasttonoise ratio of the acidoCEST technique should allow future studies to use a thinner slice thickness that can lead to a more tissueselective ROI. The improved resolution of acidoCEST MRI can also facilitate spatial registration with histology results, and can also facilitate investigations that correlate quantitative acidoCEST MRI with quantitative histopathology. Future studies would also be facilitated by using an alternative species with a larger pancreas, such as a rat, to improve the localization of pancreatic lesions.

Progression of PDAC in the untreated KC mice occurred faster than anticipated. While previous characterizations of the model suggested that PanIN lesions would first appear at 8 weeks in this model [32], we found that pancreatic tumors had developed in the untreated KC mice as early as 5 weeks. Fortunately, the timing of our acidoCEST MRI studies still captured the lower pHe during the development of the pancreatic tumors in this model. Interestingly, the average pHe was lower for the first 48 h after caerulein treatment of the KC model relative to the other models (except for the 48h time point of the caeruleintreated wildtype mice), which may indicate that the level of inflammation caused by caerulein may be higher in KC mice. Future studies should consider characterizing the level of caeruleininduced inflammation at earlier time points to better understand how inflammation affects the development of tumors in various mouse models of pancreatic cancer.

Conclusions

AcidoCEST MRI was able to measure the pHe of the pancreas and tumor tissues during progression of pancreatitis to pancreatic cancer in a caeruleintreated KC model. Pancreatic tumors had lower pHe than the pancreatitis. However, pHe could not differentiate between pancreatitis that did or did not progress to pancreatic cancer. Therefore, acidoCEST MRI is a promising technique for improving the specificity of distinguishing cancer from inflammation, but may not be able to prognosticate future development of cancer in patients with pancreatitis.

Acknowledgements

The authors thank Experimental Mouse Shared Resource of the University of Arizona Cancer Center for their assistance. This research was supported by the National Institutes of Health grant numbers P30CA23074 and P30CA016672.

Appendix A. Supplementary data

Supplementary data to this article can be found online at https://doi.org/10.1016/j.neo.2019.09.004.

References

1. Ilic M, Ilic I. Epidemiology of pancreatic cancer. *World J Gastroenterol* 2016;**22**(44):9694–705. https://doi.org/10.3748/wjg.v22.i44.9694.
2. Yadav D, Lowenfels AB. The epidemiology of pancreatitis and pancreatic cancer. *Gastroenterology* 2013;**144**(6):1252–61. https://doi.org/10.1053/j.gastro.2013.01.068.
3. Yadav D, Timmons L, Benson JT, Dierkhising RA, Chari ST. Incidence, prevalence, and survival of chronic pancreatitis: a population-based study. *Am J Gastroenterol* 2011;**106**(12):2192–9. https://doi.org/10.1038/ajg.2011.328.
4. Kramer-Marek G, Gore J, Korc M. Molecular imaging in pancreatic cancer - a roadmap for therapeutic decisions. *Cancer Lett* 2013;**341**(2):132–8. https://doi.org/10.1016/j.canlet.2013.08.008.

5. Ansari D, Gustafsson A, Andersson R. Update on the management of pancreatic cancer: Surgery is not enough. *World J Gastroenterol* 2015;**21** (2111):3157–65. https://doi.org/10.3748/wjg.v21.i11.3157.
6. Uomo G, Rabitti PG. Chronic pancreatitis: relationship to acute pancreatitis and pancreatic cancer. Ann Ital Chir 2000;71(1):17–21.
7. Dte P, Hermanova M, Trna J, Novotny I, Ruzica M, Liberda M, Bartkova A. The role of chronic inflammation: chronic pancreatitis as a risk factor of pancreatic cancer. *Dig Dis* 2012;**30**(3):277–83. https://doi.org/10.1159/000336991.
8. Li S, Tian B. Acute pancreatitis in patients with pancreatic cancer: timing of surgery and survival duration. *Medicine (Baltimore)* 2017;**96**(3). https://doi.org/10.1097/MD.0000000000005908 e5908.
9. Kirkegrd J, Cronin-Fenton D, Heide-Jrgensen U, Mortensen FV. Acute pancreatitis and pancreatic cancer risk: a nationwide matched-cohort study in Denmark. *Gastroenterology* 2018;**154**(6):1729–36. https://doi.org/10.1053/j.gastro.2018.02.011.
10. Carrire C, Young AL, Gunn JR, Longnecker DS, Korc M. Acute pancreatitis markedly accelerates pancreatic cancer progression in mice expressing oncogenic Kras. *Biochem Biophys Res Commun* 2009;**382**(3):561–5. https://doi.org/10.1016/j.bbrc.2009.03.068.
11. Munigala S, Kanwal F, Xian H, Scherrer JF, Agarwal B. Increased risk of pancreatic adenocarcinoma after acute pancreatitis. *Clin Gastroenterol Hepatol* 2014;**12**(7):1143–1150.e1. https://doi.org/10.1016/j.cgh.2013.12.033.
12. Tummala P, Tariq SH, Chibnall JT, Agarwal B. Clinical predictors of pancreatic carcinoma causing acute pancreatitis. *Pancreas* 2013;**42**(1):108–13. https://doi.org/10.1097/MPA.0b013e318254f473.
13. Corbet C, Feron O. Tumour acidosis: from the passenger to the drivers seat. *Nat Rev Cancer* 2017;**17**(10):577–93. https://doi.org/10.1038/nrc.2017.77.
14. Warburg O. On the origin of cancer cells. *Science* 1956;**123**(3191):309–14. https://doi.org/10.1126/science:123.3191.309.
15. Vander Heiden MG, Cantley LC, Thompson CB. Understanding the Warburg effect: the metabolic requirements of cell proliferation. Science 2009;324 (5930):1029–1033. DOI: 10.1126/science.1160809.
16. Zhang X, Lin Y, Gillies RJ. Tumor pH and its measurement. *J Nucl Med* 2010;**51**(8):1167–70. https://doi.org/10.2967/jnumed.109.068981.
17. Cruz-Monserrate Z, Roland CL, Deng D, ARumugam T, Moshnikova A, Andreev AO, Reshtnyak YK, Logsdon CD. Targeting pancreatic ductal adenocarcinoma acidic microenvironment. Sci Rep 2014;4:1806–1818. DOI: 10.1038/srep04410.
18. Chen LQ, Pagel MD. Evaluating pH in the extracellular tumor microenvironment using CEST MRI and other imaging methods. *Adv Radiol* 2015;**2015**. https://doi.org/10.1155/2015/206405 206405.
19. Chen LQ, Randtke EA, Jones KM, Moon BF, Howison CM, Pagel MD. Evaluations of tumor acidosis within vivo tumor models using parametric maps generated with acidoCEST MRI. *Mol Imaging Biol* 2015;**17**(4):488–96. https://doi.org/10.1007/s11307-014-0816-2.
20. Jones KM, Randtke EA, Yoshimaru E, Howison CM, Chalasani P, Klein RR, Chambers SK, Kuo PH, Pagel MD. Clinical translation of acidosis measurements with acidoCEST MRI. *Molec Imaging Biol* 2017;**19** (4):617–25. https://doi.org/10.1007/s11307-016-1029-7.
21. Chen LQ, Howison CM, Jeffery JJ, Robey IF, Kuo PH, Pagel MD. Evaluations of extracellular pH within in vivo tumors using acidoCEST MRI. *Magn Reson Med* 2014;**72**(5):1408–17. https://doi.org/10.1002/mrm.25053.
22. Moon BF, Jones KM, Chen LQ, Liu P, Randtke EA, Howison CM, Pagel MD. A comparison of iopromide and iopamidol, two acidoCEST MRI contrast media that measure tumor extracellular pH. *Contrast Media Molec Imaging* 2015;**10**(6):446–55. https://doi.org/10.1002/cmmi.1647.
23. Randtke EA, Granados JC, Howison CM, Pagel MD, Crdenas-Rodrguez J. Multislice CEST MRI improves the spatial assessment of tumor pH. *Magn Reson Med* 2017;**78**(1):97–106. https://doi.org/10.1002/mrm.26348.
24. Chen LQ, Howison CM, Spier C, Stopeck AT, Malm SW, Pagel MD, Baker AF. Assessment of carbonic anhydrase IX expression and extracellular pH in B-cell lymphoma cell line models. *Leukemia Lymphoma* 2015;**56**(5):1432–9. https://doi.org/10.3109/10428194.2014.933218.
25. Akhenblit PJ, Hanke NT, Gill A, Persky DO, Howison CM, Pagel MD, Baker AF. Assessing metabolic changes in response to mTOR inhibition in a Mantle cell lymphoma xenograft model using acidoCEST MRI. *Mol Imaging* 2016;**15**:1–10. https://doi.org/10.1177/1536012116645439.
26. Jones KM, Randtke EA, Howison CM, Pagel MD. Respiration gating and Bloch fitting improve pH measurements with acidoCEST MRI in an ovarian orthotopic tumor model. *Proc SPIE* 2016;**9788**. https://doi.org/10.1117/12.2216418 978815.
27. Lindeman LR, Randtke EA, High RA, Jones KM, Howison CM, Pagel MD. A comparison of exogenous and endogenous CEST MRI methods for evaluating in vivo pH. *Magn Reson Med* 2018;**79**(5):2766–72. https://doi.org/10.1002/mrm.26924.
28. Goldenberg JM, Crdenas-Rodrguez J, Pagel MD. Preliminary results that assess metformin treatment in a preclinical model of pancreatic cancer using simultaneous [18F]FDG PET/MRI and acidoCEST MRI. *Molec Imaging Biol* 2018;**20**(4):575–83. https://doi.org/10.1007/s11307-018-1164-4.
29. Rosembaum SJ, Lind T, Antoch G, Bockisch A. False-positive FDG PET uptake—the role of PET/CT. *Eur Radiol* 2006;**16**(5):1054–65. https://doi.org/10.1007/s00330-005-0088-y.
30. Wu C, Li F, Niu G, Chen X. PET imaging of inflammation biomarkers. *Theranostics* 2013;**3**(7):448–66. https://doi.org/10.7150/thno.6592.
31. Gurra C, Schuhmacher AJ, Caamero M, Grippo PJ, Verdaguer L, Prez-Gallego L, Dubus P, Sandgren EP, Barbacid M. Chronic pancreatitis is essential for induction of pancreatic ductal adenocarcinoma by K-ras oncogenes in adult mice. *Cancer Cell* 2007;**11**(3):291–302. https://doi.org/10.1016/j.ccr.2007.01.012.
32. Westphalen CB, Olive KP. Genetically engineered mouse models of pancreatic cancer. *Cancer J* 2012;**18**(6):502–10. https://doi.org/10.1097/PPO.0b013e31827ab4c4.